SENSITIVITY AND PROBABILISTIC ANALYSES OF THE IMPACT OF CLIMATIC CONDITIONS ON THE INFILTRATION RATE IN A VARIABLY SATURATED MULTILAYERED GEOLOGIC MEDIUM

A. Berge Gureghian, Aaron R. DeWispelare, and Budhi Sagar
Center for Nuclear Waste Regulatory Analyses
6220 Culebra Road
San Antonio, Texas 78228-0510

ABSTRACT

The performance of a high-level waste (HLW) repository in a variably saturated geologic medium can be highly influenced by the infiltration process, which in turn is affected by the climatic conditions, likely to prevail at the site in the future. This paper presents a first-order reliability analysis of a hypothetical HLW subterranean repository located in a layered, and variably saturated medium. The flow rate expressed in terms of specific discharge (SD) passing a specific point in space is selected as the performance measure to be estimated. A new one-dimensional analytical model designed to solve the quasi-linear form of Richard's equation for a multi-layered geologic medium is used to compute the performance measure, including its first order sensitivities with respect to selected parameters. The model accounts for the spatially dependent initial distribution of pressure, and handles time dependent boundary conditions represented by exponential and simple harmonic functions. A first-order reliability method (FORM) is used to estimate the probability of exceeding (or not exceeding) the specified performance measure. In addition, an estimate of the sensitivity of the stochastic solution to a select number of random variables is also reported. Climatic data produced by an expert judgement elicitation exercise is used to estimate the model boundary conditions at the surface. The reported example illustrates a possible approach for estimating the infiltration in a two-layered geologic medium, resulting from anticipated changes in climatic conditions.

INTRODUCTION

The NRC is developing methods to determine compliance with its regulation for the disposal of nuclear HLW (10 CFR Part 60) by the U.S. Department of Energy (DOE). Recent results from the U.S. Nuclear Regulatory Commission (NRC) Iterative Performance Assessment (IPA), Phase 2, indicate that repository performance in partially saturated media is highly sensitive to rates of infiltration. This paper presents preliminary investigation methods that may be useful for estimating infiltration from climatic data.

As an extension to IPA, Phase 2, the NRC also conducted an exercise in expert elicitation on future climate in the vicinity of the proposed Yucca Mountain repository. Results of this elicitation are being presented at this meeting.[1] The subjective data so obtained includes future precipitation and temperature estimates and their associated probabilities. This data will be used to demonstrate the method described in this paper.

In addition to climatic conditions, infiltration rates depend upon the site topography and subsurface hydrological conditions. The bedded tuff site at Yucca Mountain incorporates several complex structural/tectonic features that will influence the infiltration rate. As a first step towards studying the sensitivity of the performance measure (SD) to several key system parameters related to climate and geohydrology over a period of 10,000 years, a simplified conceptual model was adopted. The flow domain located in the vadose zone, is simulated by an idealized semi-infinite vertical column of a geologic medium, which included two parallel layers of rocks. For such a case, an analytic solution[2] for the nonsteady flow of groundwater has been derived. Coupled with time-varying expressions of precipitation and evapotranspiration, the analytical solution for the quasi-linearized flow equation in an unsaturated medium is then used, to estimate the infiltration rate. In spite of modeling limitations of analytic solutions, their high degree of precision and computational efficiency make them suitable for exploring some of the critical uncertainties inherent in the infiltration process.

In this paper, presentation of analysis method is stressed over application to any specific site. We shall report: (i) equations governing the vertical movement of water in a variably saturated geologic medium, including the procedure incumbent to their linearization, (ii) selected model for estimating evapotranspiration and handling the climatic data (i.e., temperature, cloud cover and other atmospheric parameters) generated by the expert elicitation exercise, (iii) the uncertainty and sensitivity methods, and finally, (iv) a test case of infiltration in a variably saturated layered rock system, to demonstrate the salient features of the proposed approach.

GOVERNING EQUATIONS

The vertical flux (q) component for water in porous media under laminar and isothermal flow conditions is given by Darcy's law as follows

$$q = - K(h)(\frac{\partial h}{\partial z} - \frac{\partial z}{\partial z}) \qquad (1)$$

where

K = hydraulic conductivity (K_s, K_r)
K_s = saturated hydraulic conductivity (LT^{-1})
K_r = the relative hydraulic conductivity
h = pressure head $(p/\rho g)$ (L)
p = fluid pressure $(ML^{-1}T^{-2})$
ρ = fluid density (ML^{-1})
g = acceleration of gravity (LT^{-2})
z = elevation from datum (i.e., earth surface) taken positive downwards (L)

The governing equation describing transient-state groundwater flow in a vertical column of partially saturated porous rock, in the absence of sources or sinks, as reported by Richards[3] is given by

$$\frac{\partial \theta}{\partial t} = \frac{\partial}{\partial z}\left(K(h)\frac{\partial h}{\partial z}\right) - \frac{\partial K(h)}{\partial z} \qquad (2)$$

where θ is the volumetric moisture content (L^3L^{-3}), and t is the time. Note that Eq. (2) is highly nonlinear, but will be linearized for this study.

Adopting the nonhysteretic functional model of the hydraulic conductivity curve as proposed by Gardner[4] written as

$$K(h) = \begin{cases} K_s \exp[\alpha(h - h_0)] \, , & h \leq h_0 \\ K_s \, , & h > h_0 \end{cases} \qquad (3)$$

where h_0 and α (L^{-1}) in Eq. (3) correspond to the bubbling pressure head, and a constant dependent upon the pore structure of the rock matrix, respectively. Furthermore, defining a matrix flux potential ϕ (L^2T^{-1}) as

$$\phi = \int_{-\infty}^{h} K(h)dh \qquad (4)$$

Eqs. (1) and (2) are then transformed[5] to

$$q = - \frac{\partial \phi}{\partial z} + \alpha\phi \qquad (5)$$

$$\frac{\partial \phi}{\partial t} = \left(\frac{k}{\alpha}\right)\frac{\partial^2 \phi}{\partial z^2} - k\frac{\partial \phi}{\partial z} \qquad (6)$$

where $k = dK/d\theta$, whereas k/α corresponds to the moisture diffusivity $D = K(dh/d\theta)$ (L^2T^{-1}) assumed to be constant in this study. Note that Eq. (6) is still nonlinear, and consequently some average value for the diffusivity is required. The diffusivity function is represented by the empirical nonhysteretic form[6]

$$D(\theta) = D_o \exp(\beta_o \theta) \qquad (7)$$

where D_o (L^2T^{-1}) and β_o (L^3L^{-3}) are specified constants obtained by curve fitting the above equation to experimental data D versus θ. The weighted average diffusivity model[7] and written as

$$\bar{D} = \int \theta^2 D(\theta)d\theta \qquad (8)$$

is then used to get a constant value for use in Eq. (6), where the integration is performed over the range of moisture contents of interest. The diffusivity values used in the investigated problem will be given in a subsequent section of this paper. It may be easily shown that

$$\frac{d\theta}{d\phi} = \frac{1}{D} \qquad (9)$$

and integrating the above relation within its appropriate limits, would then yield the functional model of the moisture content given by

$$\theta = \frac{1}{D}\left(\phi - \phi_r\right) + \theta_r \, , \quad h \le h_0 \tag{10}$$

$$\theta = \theta_s \, , \quad h > h_0$$

where subscripts r and s refer to the residual and saturated value of the pressure head.

Initial and Boundary Conditions

The initial condition written in terms of the pressure head is assumed to be a linear function of the vertical coordinate z. For the ith layer, we have

$$h_i(z,0) = a_i(z - Z_{i-1}) + h_{i_{R_i}} \tag{11}$$

where Z_i is the depth of the interface between consecutive layers measured from datum, and a_i (L^{-1}) and $h_{i_{R_i}}$ (L) are layer dependent constants. Note that for the last layer say n, a_n must be negative in order to comply with the boundary conditions given by Eq. (16).

The corresponding initial condition expressed in terms of the matrix flux potential is given by

$$\phi_{r_i}(z,0) = \int_{-\infty}^{h_i(z,0)} K_{s_i} \exp\left[\alpha_i\left(h - h_{\alpha_i}\right)\right] dh \tag{12}$$

The boundary condition at the surface subject to a time-dependent flux $Q_s(0,t)$ is given by

$$-\frac{\partial \phi_1(0,t)}{\partial z} + \alpha_1 \phi_1(o,t) = Q_s(0,t) \tag{13}$$

The selected model for the boundary condition at the earth surface representing a reasonable approximation to the precipitation and evaporation process within a 10,000 years interval, includes three typical flux components; a mean value based on current estimates, a time-dependent one describing the perturbations from the mean, and an oscillatory one describing the seasonal fluctuations. This is written as

$$Q_s(0,t) = \sum_{j=1}^{m} \sum_{i=1}^{2} (-1)^{i+1}\left[q_{s_{ij-1}}(t - T_{j-1})\, U(t - T_{j-1}) \right. \tag{14}$$
$$\left. - q_{s_{ij}}(t - T_j)\, U(t - T_j)\right]$$

where $U(\cdot)$ is the Heaviside function, and $q_{s_{ij}}$ is given by is the time dependent net prevailing flux at the earth's surface, and

$$q_{s_{ij}}(t) = \sum_{i=1}^{2} \bar{q}_{ij} + \left(q_{a_{ij}} + q_{b_{ij}} e^{-\lambda_{ij}t}\right) \tag{15}$$
$$+ q_{0_i}\sin\left(\omega_i t + \Phi_i\right), \quad z = 0$$

$\bar{q}_{ij}$ = mean value of the flux (LT^{-1})

$q_{a_{ij}}$ = curve fit initialization constant (LT^{-1})

$q_{b_{ij}}$ = curve fit accelerator constant (LT^{-1})

λ_{ij} = curve fit slope indicator (T^{-1})

q_{α_i} = the amplitude of variation (LT^{-1})

ω_i = frequency of oscillations (i.e., $2\pi/\tau$) (T^{-1})

τ = time period of a complete cycle of variation (T)

Φ_i = phase angle

T_j = time interval (T)

Subscript i refers to precipitation ($i=1$) and evaporation ($i=2$). Subscript j refers to a particular time interval of the 10,000 yr period of interest. Note that by our convention, precipitation-associated values are taken positively downwards and evapotranspiration negatively.

With the water table assumed to be very deep, the lower end boundary condition is given by

$$-\frac{\partial \phi_n(\infty,t)}{\partial z} + \alpha_n \phi_n(\infty,t) = 0 \tag{16}$$

With the flux described by Eq. (5), at the interface of two consecutive rock layers we have

$$\alpha_i \phi_i(0,t) = \alpha_{i-1}\phi_{i-1}(L_{i-1},t), \quad i < n \tag{17}$$

$$\frac{\partial \phi_i(0,t)}{\partial z} = \frac{\partial \phi_{i-1}(L_{i-1},t)}{\partial z}, \quad i < n \tag{18}$$

where n corresponds to the number of rock layers.

The analytical solutions to Eqs. (5) and (6) subject to their initial and boundary conditions, including the continuity requirement relation at the interface between successive layers were obtained through a Laplace transformation technique[2] where the superposition theorem was used to cope adequately with the time-dependent boundary conditions given by Eq. (14). The closed-form solution for a single rock layer was extended to a multi-layered system (i.e., n layers) through the successive application of the convolution theorem, requiring a multiple evaluation of $(n-1)$ integrals performed through a Gauss-Legendre integration scheme.

CLIMATIC CONSIDERATIONS

Performance of HLW geologic repositories has to be assessed for a regulatory period of 10,000 years (40 CFR Part 191). Because of this extremely long period, a combination of data from site characterization, experimental methods, studies of natural analogs, and mathematical models will be used in performance assessments (PAs). Mathematical models are expected to be the primary tools for estimating the long-term future performance of the repository. Some data gathered for this project will require interpretation and supplementation before it can be incorporated into these mathematical models. Expert judgment elicitation is a potential source of this data interpretation and supplementation.

The NRC sponsored an expert judgment elicitation exercise focused on future climate in the vicinity of Yucca Mountain Nevada (YMNV). Detailed description of this elicitation is presented in a published report.[8] Five climatologists predicted the future climate at YM.

Precipitation

The individual experts' predictions were aggregated for temperature, precipitation, and cloud cover changes over 10,000 after present (AP) with the results shown in Figure 1a, b, and c. These curves represent the median values of a set of probability distributions which were elicited for the 100, 300, 1,000, 3,000, 5,000, 7,500, and 10,000 yr future time epochs. The median value trend curves shown in Figure 1 were broken up into segments which could be characterized by a set of linked piecewise models which adhere closely to the mathematical form shown in equation (15). Using standard regression techniques, these curves and associated probability distributions for temperature and precipitation were parameterized. The data for precipitation is shown in Table 1A. The correlation coefficient of determination (r^2) was greater than 0.99 for all piecewise segments shown in Table 1A. Seasonal data (average variation over a year) is also included for precipitation and temperature. These curves represent changes (the median of distributions of 100 year moving averages) to the current conditions in the vicinity of YM (14 °C average temperature and 150 mm average annual precipitation). The aggregation of the data curves (median values of the distributions of the time epochs) were averaged using equal weighting to produce the curves shown in Figure 1a, b, and c. Up to 10 yr AP, the current conditions are predicted to continue. Variations from present conditions are plotted for the period following the next decade in Figure 1.

Evapotranspiration

Evaporation modeled under isothermal conditions neglects the influence of the vertical flux in the soil due to thermal gradients, and would yield a rough approximation to a very complicated process.[9,10] Furthermore, because of the limitations of our analytical model to handle nonlinear boundary conditions, resulting from the dependence of the evaporative flux on the pressure head, an alternative solution was sought. It was first assumed that a light vegetative cover existed at the surface of the site under investigation, and a viable formula for predicting the evapotranspiration (i.e., the combined process of evaporation and transpiration) rate was selected. Among the large number of existing formulae for estimating potential evapotranspiration rate based on a combination of meteorologic data, the one reported by Penman[11] was adopted here, primarily because it combines adequately both surface energy balance and aerodynamic theory, to predict a relationship between evapotranspiration E_t and meteorologic data, not to mention that this formula has been applied with a great deal of success. The basic equations are given by

$$E_t = f E_o \qquad (19a)$$

$$E_o = \frac{\Delta H + \gamma E_a}{\Delta + \gamma} \qquad (19b)$$

where

E_o = evaporation rate from a water surface

f = a reduction factor depending on the month of the year

Δ = slope of saturation vapor pressure curve at surface temperature T_s (mm. Hg/°C)

γ = psychrometric constant (mm. Hg/°C)

H = the net radiation ($H = R_s - R_l$) (cal/cm^2/day), with R_s and R_l corresponding to the incoming short-wave and outgoing long-wave solar radiation fluxes at the surface, written as

$$R_s = (1 - r) R_a \left(0.18 + 0.55 \frac{n}{N} \right) \qquad (20)$$

$$R_l = \sigma T_s^4 \left(0.56 - 0.092 \sqrt{e_d} \right) (1 - 0.9m) \qquad (21)$$

where

R_a = Angot value of maximum possible radiation

r = albedo of surface

n/N = duration of bright sunshine per day/possible duration

m = fraction of sky covered by clouds ($1-m= n/N$)

σT_s^4 = black body radiation at mean surface temperature T_s (cal/cm^2/day)

σ = Stephan Boltzman's constant

e_d = saturation vapor pressure at mean dew point (mm. Hg)

Finally, the aerodynamic component of evaporation assuming the soil surface to be at air temperature. is given by

$$E_a = 0.35\left(e_s - e_d\right)\left(1 + U_2/100\right) \qquad (22)$$

where

e_s = saturation vapor pressure at mean air temperature (mm. Hg) $(e_d = e_s \bar{h}_a)$

$\bar{h}_a$ = relative humidity of air

U_2 = mean wind velocity at 2m above ground (miles/day)

With the site located at a latitude of 36.4° in the Northern hemisphere, the monthly values for R_a were obtained by linear interpolation using data reported by Shaw.[12] The values assigned to f in Eq. (19a) correspond to: 0.6 from November to February, 0.4 from May to August, and 0.7 for the remaining four months, converging to an overall mean of 0.57. Note that the ad hoc 50 percent reduction imposed on f for the summer months (i.e., May to August), reduced by 18.5 percent the original value of 0.7 proposed by Penman[11] for humid regions (i.e., southeast England). This however, seems quite in line with his suggestions, that smaller values of f may be more appropriate for semi-arid regions. The percentage reflection or Albedo r, which is dependent on the nature of the surface. the angle of the sun, and the solar elevation was assigned a value of 0.36 from May to October, and 0.27 for the remaining months.[13]

Based on remarks raised by Philip[14] and Staple[15] the earth surface temperature T_s was substituted for the air temperature T_a in the original formula. and estimated after a linear relation proposed by Staple,[15] written as

$$T_s = 1.1\, T_a + 0.17 \qquad (23)$$

which has also been used to estimate the slope Δ of the e_s:T_s function. The e_a:T_a function is represented by the empirical relationship[16]

$$e_a = 7.5 \exp\left[52.576 - \left(\frac{6790.5}{T_a}\right) - 5.028 \ln\left(T_a\right)\right] \qquad (24)$$

where the units of e_a and T_a are in mm. Hg and °K respectively.

The time-dependent values of T_a, and m for the period of interest were based on the ones reported in Figures 1b and 1c. The monthly average values of T_a, $\bar{h}_a$, and U_2 reported in SCP,[17] which led us to determine the monthly perturbations effects of evapotranspiration, were assumed time invariant.

UNCERTAINTY ANALYSIS

The reliability approach for estimating probabilities associated to groundwater flow and solute transport appears to have attractive computational features[18,19] compared to other standard methods such as Latin Hypercube or Monte Carlo simulation, particularly for low probability events. In addition, the reliability method allows an easy evaluation of the probabilistic sensitivities of the performance measure to changes in the individual parameters of interest.

With the performance function defined as $Z = g(X)$ where X is a vector of n random variables, by convention the event of interest is said to occur when $g(X) \le 0$, denoting the failure event. The hyper-surface defined by $g(X) = 0$, known as the limit state surface denotes the boundary between the "safe" and "failure" regions (see Figure 2a). If as in the present case one is seeking the probability, that for example the specific discharge will exceed a selected target value q_o at a particular point in space and time, the performance function will then be formulated as $g(X) = q_o - q$. The probability of failure is given by

$$P[g(X) \le 0] = \int\limits_{g(X) \le 0} f_x(x)\, dx \qquad (25)$$

where $f_x(x)$ is the joint pdf of X. The joint pdf's of X are seldom known, whereas the numerical integration of the resulting multifold integral would be quite cumbersome. Because of these difficulties the FORM would provide an alternative means for obtaining an approximate evaluation of the above integral.

In the reliability approach the random variables X with mean M [μ_i] are transformed to standard normal uncorrelated variables through a linear transformation written as

$$Y = L^{-1} D^{-1} (X - M) \qquad (26)$$

where D diag[σ_i] is a diagonal matrix of the standard deviations, and L is the lower triangular matrix obtained from the decomposition of the correlation matrix R [ρ_{ij}]; i.e, $=LL^T$. Using the inverse transformation $X = M + DLY$,

the expression for the limit surface (see Figure 1b) is given by

$$g(x) = g(M + DLY) \equiv G(y) \qquad (27)$$

The calculation of the reliability index reported later in this section, requires the determination of the nearest point on the limit state surface to the origin in the standard space. The reliability index[20], β (i.e., the distance to the failure surface), is given by

$$y^* = \beta \, \alpha^* \qquad (28)$$

where y^* is the solution for y at the design point and α^* (see Figure 2b) corresponds to the gradient of the vector at that very same point, directed towards the unsafe region.

In this paper, the marginal PDF and first and second statistical moments are assigned to each uncertain variable, which have either normal or lognormal marginal distributions. Note that in the latter case, the linear transformation given in Eq. (26) no longer applies,[21] since the transformation is nonlinear, and is given in terms of the joint distribution[22] of X.

At each step of the iterative algorithm used to determine the design point y^*, the values of the first two moments for the non-normal variables are constantly updated. As before, the uncertain correlated variables (X) are transformed into a set of uncorrelated standard normal variates $Y = \Gamma_o Z$, where Z is a vector of correlated standard normal variates obtained by $Z_i = \Phi^{-1}[F_{x_i}(x_i)]$, and Γ_0 is the lower triangular matrix obtained from the decomposition of the correlation matrix of the Z variables. Φ (·) is the standard normal integral, the superscript -1 denotes the inverse function, where $F_{x_i}(x_i)$ is the cumulative distribution function (CDF) of the x_i's. A set of relations between the correlation coefficients for the standard normal Z variables and the correlation coefficients for the X variables, were established through an integral relation given by Der Kiureghian and Liu,[22] who provided tables for selected marginal distribution pairs.

For a nonflat limit surface, the search for the Hasofer-Lind[20] reliability index β requires an iterative procedure. The algorithm used here is based on Rackwitz and Fiessler.[23] which yields a sequence of points $y_1, y_2 \cdots, y_n$ in the standard space according to the rule

$$y_{i+1} = \left[y_i^T \alpha_i + \frac{G(y_i)}{|\nabla G(y_i)|} \right] \alpha_i \qquad (29)$$

where

$$\nabla G(y) = \left[\frac{\partial G(y)}{\partial y_1}, \dots, \frac{\partial G(y)}{\partial y_n} \right]^T$$

is the gradient vector, which expressed in terms of the gradient vector in the original space, is given by

$$\nabla G(y) = \Gamma_o R_o D \, \nabla g(x) \qquad (30)$$

and the vector of direction cosines is given by

$$\alpha = -\frac{\nabla G(y)}{|\nabla G(y)|} \qquad (31)$$

Once convergence to y^* and α^* to the preset criteria is achieved, the reliability index is then computed from

$$\beta = |y^*| \qquad (32)$$

and subsequently the design point y^* is then transformed back to its counterpart in the original space x^*, in order to reflect its physical significance. A first order approximation to Eq. (25) is given by

$$P[g(x) \leq 0] \approx \phi(-\beta) \qquad (33)$$

Note that the approximation in the above equation is first order exact when a marginal PDF for each X uncertain variable is available. Moreover under certain circumstances e.g., highly nonlinear problems, second order approximations[24] are required. Further discussions on this issue are beyond the scope of this paper.

Nothing has been mentioned so far, about the initial guessed values for y in the iteration process, nor the selection of target values for the performance measure. Initial guesses for y would correspond either to zero or the mean value x, as long as the target value of the performance measure remains close to its mean. In this context, a first estimate of the target value corresponding to some selected CDF values, may be obtained from the MVFOSM (mean value first order second moment) algorithm.[25] where the gradient vector is evaluated at the mean point. About nine evaluations of the performance measure may adequately capture the approximate CDF profile. The values of the x variables computed at these points on the CDF might provide useful initial guesses for the transformed variables y in critical regions of the CDF.

Sensitivity Measures

Probabilistic sensitivity measures which provide information regarding anticipated changes that might be expected given changes in some of the statistical information are a vital complement to the uncertainty analysis. These are obtained at no extra computational effort, since the components entering their evaluation are the ones required by the preceding uncertainty analysis.

A sensitivity measure in the space of the original random variables proposed by Der Kiureghian and Liu,[26] which estimates the sensitivities of the reliability index β to standard variations in the uncertain parameters (X) is given by

$$\gamma = \frac{\Gamma_o^T \alpha}{|\Gamma_o^T \alpha|} \qquad (34)$$

Physically the probabilistic sensitivity measures will, in addition to the deterministically derived sensitivities, rely upon the marginal distributions, the magnitude of the standard deviation, correlation and nature of the surface $G(Y)=0$ near the design point y^*.

In this instance the components of the gradient vector, $\nabla G(y)$, corresponding to the deterministic sensitivities have been calculated by a backward difference finite-difference scheme.

RESULTS

The potential evaporation for the succeeding 10,000 yr were computed using Penman's equation. The mean annual value obtained was 144 mm potential evapotranspiration. The average variation over 10,000 yr is plotted in Figure 1d. Breaking this curve into the same intervals as previously done with precipitation, temperature, and cloud cover, and statistically regressing each piecewise segment to the model form of equation (15), produced the results shown in Table 1B. Again, the r^2 values were in excess of 0.99 for each of the six segments.

The test case reported here addresses one-dimensional transient infiltration of water in a two-layered geologic medium, where the first layer has a finite thickness L_1, and the second extends to infinity. The first layer is assumed to be more permeable than the second, yielding a coarse-fine (CF) structural stratification. The triggering effect of the infiltration process is restricted to predicted changes in climatic conditions, with no consideration of the surface runoff process. The porous rock layers are assumed to exhibit residual initial pressures at the onset of infiltration, described by a linear function of space in the case of the

first layer and by a constant in the second. Time dependent fluxes (i.e., precipitation and evapotranspiration) described by Eq (14), which are likely to prevail at the earth surface over the next 10,000 years, represent the surface boundary conditions. The input data related to the climatic and hydrogeologic parameters are given in Table 1 and Table 2.

Figure 3a reports a comparison of the spatial variations of the pressure head due to the seasonal and annual fluctuations of the climatic parameters, obtained at four observation times corresponding to 100, 1000, 5,000 and 10,000 years after present (AP). In this paper, seasonal fluctuations of the climatic parameters correspond to the combination of the first and last terms on the right hand side of Eq. (15). The annual fluctuations correspond to the entire Eq. (15). Results indicate that the difference in the rate of advance of the wetting front due to these two climatic variation modes is minimal, however the gradient of these profiles exhibits more stability in the case of the seasonal variations. Note that at 100 years, the wetting front has just progressed beyond the interface of the two layers, whereas migration depths corresponding to 35m, 112m and 200m from the surface are registered for the remaining three observation times. The progression rate of the wetting front is a nonlinear function of time, initially high but progressively slowing down past the 10^3 years mark strongly influenced by the impeding properties of the fine layer.

Figure 3b illustrates the spatial variations of the specific discharge (i.e, Darcy velocity) for the four observation times. Of interest are the profiles at 5,000 and 10,000 years, which magnify the gradient perturbations. These are a direct consequence of the large climatic changes predicted for the period of interest.

Figures 4a and 4b illustrate the temporal variations of the specific discharge (SD) due to the two climatic variation modes, recorded at two observation points, where the first is located at the interface of the two rock layers and the second in the fine layer, corresponding to depths of 10m and 25m, respectively. Results show that the perturbation effects due to seasonal variation of the surface fluxes seem to vanish with increasing time, yielding a smooth profile where the value of the flux becomes asymptotic to one corresponding to 6×10^{-3} m/year. The perturbation of the fluxes in the case of the annual variation, recorded at time intervals three and five (see Table 1A) seems most prominent in the case of the first observation point.

Figures 5a and 5b illustrate the temporal variation of the deterministic sensitivity of flux to trend parameters λ_{1j} and λ_{2j}, for the range of time intervals j, associated to precipitation and evapotranspiration as reported in Table 1A and 1B. Results indicate that the flux is sensitive to values

restricted to intervals four, five and six in both cases. The most important rate parameters were the ones associated with interval four in both cases. This can be attributed to the increasing precipitation rate beyond 1,000 years AP.

With SD selected as the performance measure at an observation point located at 10m from the surface, the reported reliability methods are then applied, to estimate the uncertainty and sensitivity for exceeding some specified targets. In this instance, the uncertain parameters are assumed to be statistically independent, in which case the correlation matrix R is reduced to a unit diagonal matrix. The saturated hydraulic conductivity is assumed to have a marginal pdf of lognormal form, whereas the remaining parameters are assigned a normal pdf. A coefficient of variation (CV = σ/μ) of 0.2 is assigned to all parameters with the exception of the climatic trend rates, which have distinct coefficients of variation as given in Tables 1A and 1B. Note that the group of trend parameters λ_1 and λ_2, which did not show any significant impact on the performance measure in the reported deterministic sensitivity analysis, were not considered here. The total number of random variables examined for probabilistic analysis in this instance was 45.

Figure 6a shows the probability that SD would exceed selected CDF target values of q_o at time corresponding to 10,000 years. The first approximation for nine CDF values was based on the MVFOSM, and an improvement of the former solution was achieved through the FORM approach, where only five target values of q_o corresponding to $\phi(\beta_{MVFOSM})$, with β_{MVFOSM} taken as -4, -3, 0, 3 and 4 were selected for the purpose. Note that on average four iterations per target value were required by the FORM to meet our convergence criterion, set to correspond to a 1% relative change in the value of β_{FORM} observed in two successive iterations.

Figure 6b shows the probabilistic sensitivity measures γ [see Eq. (34)] for the first six most important random variables $K_{s_1}, \bar{q}_{16}, \bar{q}_{26}, q_{b_{13}}, q_{a_{16}}, q_{b_{16}}$ computed at two selected CDF points (0.000281 and 0.9998) corresponding to the tail regions (i.e., $q_o = -1.30 \times 10^{-2}$ m/yr and $q_o = 1.68 \times 10^{-2}$ m/yr). This importance was based on $\phi(\beta_{MVFOSM} = 0)$ where $q_o = 1.87 \times 10^{-3}$ m/yr, results of which are plotted in Figure 6b. The results indicate that an exclusive reliance on the latter may lead the investigator to erroneous conclusions.

SUMMARY

This paper illustrated a methodology for addressing infiltration in a one-dimensional layered variably saturated

geologic medium in response to climatic forcing. Reported were: (i) the mathematical statement of the infiltration problem, including the approach used to solve the nonlinear governing equation, (ii) a model for estimating evapotranspiration, (iii) a first order reliability method for performing the uncertainty and sensitivity analyses, and (iv) a test case of infiltration which accounted for realistic climatic and hydrogeologic data with attributes representative of the proposed HLW repository site at Yucca Mountain.

In addition to providing the CDF of the selected performance measure, the first order reliability method has proved to be a valuable asset for yielding the probabilistic sensitivities. The latter were then used to estimate the relative importance of the selected random parameters, a very useful requirement in performance assessments.

Although preliminary, these investigations have shown that the annual variations resulting from a expert judgment elicitation, have potentially significant impact on flux perturbation, but produce minor impact on the overall movement of the wetting front.

Because of the sparsity of evapotranspiration related data, lysimeter studies may be needed at the site of the proposed repository, in order to gain more insight in the actual process of evapotranspiration.

REFERENCES

1. A.R. DeWispelare, M.P. Miklas, L.T. Herren, R.T. Clemen, A.B. Gureghian, and J.R. Park. "The Use of Expert Elicitation in the Performance Assessment of the Proposed High-Level Nuclear Waste Repository." Submitted for presentation at the 1994 International High-Level Radioactive Waste Management Conference, 1993.

2. A.B. Gureghian, and B. Sagar. *INFILT: Analytical Solutions for One-Dimensional Infiltration in a Multi-Layered Variably Saturated Geologic Medium*. In preparation Center for Nuclear Waste Regulatory Analyses. San Antonio, TX (1994).

3. Richards, L.A. "Capillary Conduction of Liquids Through Porous Mediums." *Physics* 1. 318-333. (1931).

4. W.R. Gardner. "Some Steady-State Solutions of the Unsaturated Moisture Flow Equation with Applications to Evaporation from a Water Table." *Soil Sci.*, 85 (4), 228-232 (1958).

5. A.W. Warrick and D.O. Lomen, "Time-Dependent Linearized Infiltration: III. Strip and Disc Sources. *Soil Sci. Soc. Am. Proc.*, 40 (5), 639-643 (1976).

6. W.R. Gardner and M. S. Mayhugh. "Solution and Tests of the Diffusion Equation for the Movement of Water in Soil," *Soil Sci. Soc. Am. Proc.*, 22, 197-201 (1958).

7. L.D. Baver., W.H. Gardner and W.R. Gardner. *Soil Physics*, 4th Edition, John Wiley & Sons. Inc.. New York, 498 (1972).

8. A. R. DeWispelare, L.T. Herren. M.P. Miklas, and R.T. Clemen. *Expert Elicitation of Future Climate in the Yucca Mountain Vicinity.* CNWRA 93-016. Center for Nuclear Waste Regulatory Analyses, San Antonio, TX (1993).

9. J.R. Philip and D. A. de Vries. "Moisture Movement in Porous Materials Under Temperature Gradients," *Trans. Amer. Geophys. Union.* 38, 222-232 (1957).

10. C.H.M. van Bavel and D. I. Hillel. "Calculating Potential and Actual Evaporation from a Bare soil Surface by Simulation of Concurrent Flow of Water and Heat," *Agric. Meteorol.* 17, 453-476 (1976).

11. H.L. Penman. "Estimating Evaporation." *Trans. Amer. Geophys. Union*, 37, 43-50 (1956).

12. N. Shaw., *Manual of Meteorology, Vol.II, Comparative Meteorology*, 2nd edition, Cambridge University Press (1936).

13. H.G. Houghton. "On the Annual Heat Balance in the Northern Hemisphere." *J. Meteor.*, 11 1-9. (1954).

14. J.R. Philip. "Evaporation, and Moisture and Heat Fields in the Soil." *J. Meteorlog.*, 14. 354-366 (1957).

15. W. Staple, "Modified Penman Equation to Provide the Upper Boundary Conditions in Computing Evaporation from Soil." *Soil Sci. Soc. Am. Proc.*, 38, 837-839 (1974).

16. G.S. Campbell. *An Introduction to Environmental Biophysics*, p. 159. Springer-Verlag, New York (1977).

17. Department of Energy, *Site Characterization Program (SCP), Yucca Mountain Site, Vol II*, Nevada Research and Development Area, Part A, Chapter 5 (1988).

18. Wu, Y.T., A.B. Gureghian, B. Sagar and R.B. Codell. *Sensitivity and Uncertainty Analyses Applied to One-Dimensional Radionuclide Transport in a Layered Fractured Rock, Volume 2.* NUREG/CR-5917. U.S. Nuclear Regulatory Commission, Washington, DC (1992).

19. A.B. Gureghian, Y.-T. Wu, B. Sagar, and R.G. Baca. "Sensitivity and Probabilistic Analyses of Ground Water Travel Time in a Fractured and Variably-Saturated Geologic Medium." *Proceedings of the Fourth Annual International High Level Radioactive Waste Management Conference.* American Nuclear Society, LaGrange Park, IL. pp. 689-696 (1993).

20. A. M. Hasofer and N. Lind. "An Exact and Invariant First-Order Reliability Format. *J. Eng. Mech. Div. Am. Soc. Civ. Eng.*, 100, 111-121 (1974).

21. H. O. Madsen, S. Krenk and N. C. Lind, *Methods of structural safety*, p. 403. Prentice-Hall, Englewood Cliffs, N. J. (1986).

22. A. Der Kiureghian, and P-L. Liu. "Structural Reliability Under Incomplete Probability Information," *J. Eng. Mech. Am. Soc. Civ. Eng.*, 112(1), 85-104 (1986).

23. R. Rackwitz and B. Fiessler. "Structural Reliability Under Combined Random Load Sequences," *Computers and Structures. Vol. 9.*, 489-494 (1978).

24. A. Der Kiureghian, A., H.-Z. Lin, and S.-J. Hwang, "Second-Order Reliability Approximations," *J. Eng. Mech. Am. Soc. Civ. Eng.*, 113(8), 1208-1225 (1987).

25. A.H-S. Ang and W.H. Tang, *Probability Concepts in Engineering Planning and Design, Vol II: Decision, Risk and Reliability*, p. 562. J. Wiley & sons, New York, N.Y. (1984).

26. A. Der Kiureghian., and P-L. Liu. *Structural Reliability Under Incomplete Probability Information.* UCB/SESM-85/01, Div of Struct. Eng. and Struct. Mech.. Dep. of Civ. Eng., Univ. of Calif., Berkeley (1985).

Table 1. Input Climate Parameters

A. Precipitation Model $\left[\bar{q}_{1j} \cdot q_{a_{1j}} \cdot q_{b_{1j}} \exp^{-\lambda_{1j}t} \cdot q_{o_1}\sin(\omega_1 t + \phi_1) \right]$

j	Years, AP	$q_{a_{1j}}$ (m/month)	$q_{b_{1j}}$ (m/month)	λ_{1j} (m/month)	σ_{1j}/μ_{1j}
1	10-100	6.55 E-04	-1.32E-03	-4.68E-03	0.13
2	100-300	-2.64 E-04	2.27E-03	-7.58E-04	0.14
3	300-1,000	-5.25 E-05	-1.22E-04	-1.75E-04	0.15
4	1,000-5,000	3.53 E-03	-4.14E-03	-8.33E-06	0.15
5	5,000-7,500	-1.45 E-04	4.36E-04	2.50E-05	0.16
6	7,500-10,000	5.33 E-03	-8.23E03	-1.66E-05	0.14
		q_{o_1}=6.67E-04 m/month; ω_1=0.53 month^{-1}; ϕ_1=1.04 rads			

B. Evapotranspiration Model $\left[\bar{q}_{2j} \cdot q_{a_{2j}} \cdot q_{b_{2j}} \exp^{-\lambda_{2j}t} \cdot q_{o_2}\sin(\omega_2 t + \phi_2) \right]$

j	Years, AP	$q_{a_{2j}}$ (m/month)	$q_{b_{2j}}$ (m/month)	λ_{2j} (m/month)	σ_{2j}/μ_{2j}
1	10-100	1.750E-05	-1.583E-05	-6.183E-07	0.08
2	100-300	-2.108E-04	3.075E-04	3.800E-04	0.08
3	300-1,000	-2.108E-04	3.075E-04	3.800E-04	0.09
4	1,000-5,000	9.275E-04	-1.209E-03	5.708E-06	0.07
5	5,000-7,500	9.275E-04	-1.209E-03	5.708E-06	0.08
6	7,500-10,000	9.275E-04	-1.209E-03	5.708E-06	0.09
		q_{o_2}=3.58E-04 m/month; ω_2=0.53 month^{-1}; ϕ_2=1.57 rads			

Note: σ_{ij}/μ_{ij} = Coefficient of Variation for λ_{ij}, where σ_{ij} and μ_{ij} are the mean and standard deviation for parameter i in period j; $\bar{q}_{1j}$ = 1.25 × 10^{-3} m/month $\forall j$; and $\bar{q}_{2j}$ = 1.2 × 10^{-3} m/month $\forall j$

Table 2. Input parameters (hydrogeology)

i (layer)	Z_i (m)	K_{s_i} (m/month)	α_i (m^{-1})	h_{in_i} (m)	a_{ij} (m^{-1})
1	10.0	0.257	4.873	−20.0	0.5
2	∞	0.129	2.023	−15.0	0.0

i (layer)	h_{o_i} (m)	D_o (m^2/month)	β_0	θ_s	θ_r	$\bar{D}$ (m^2/month)
1	−0.1	2.59E-04	20.18	0.36	4.3E-03	1.814E-03
2	−0.1	4.49E-03	18.5	0.25	5.0E-02	1.022E-03
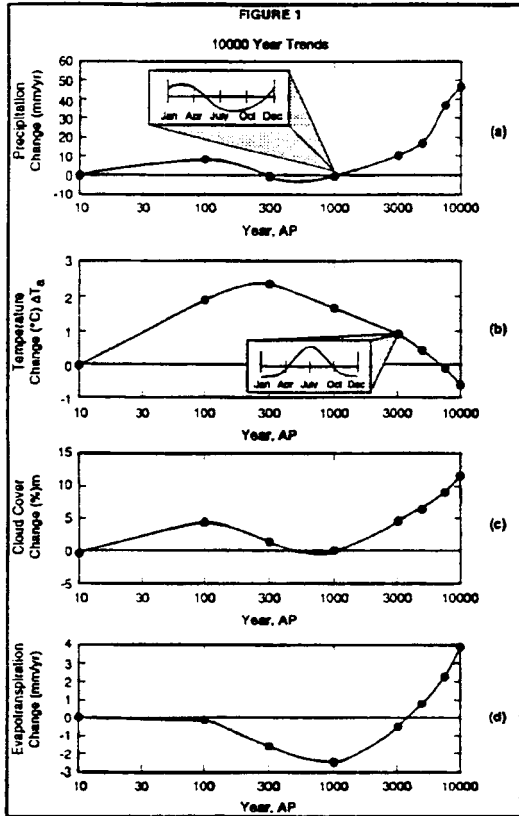
Figure 1. Climatic parameters
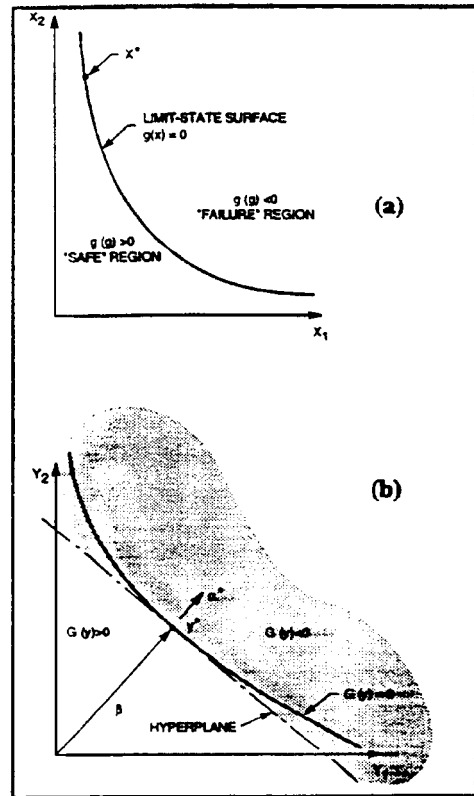
Figure 2. (a) Joint sample space
(b) Standard space
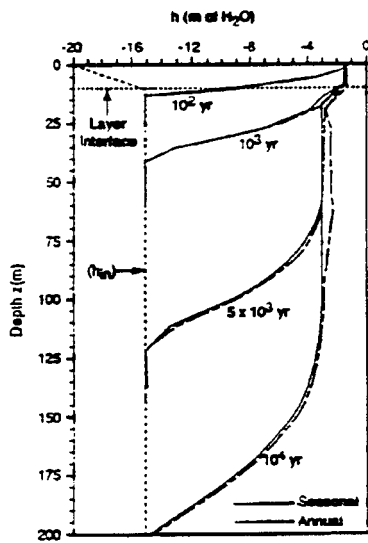
Figure 3a. Comparison of pressure head profiles at various time intervals for seasonal and annual fluctuation of climatic parameters
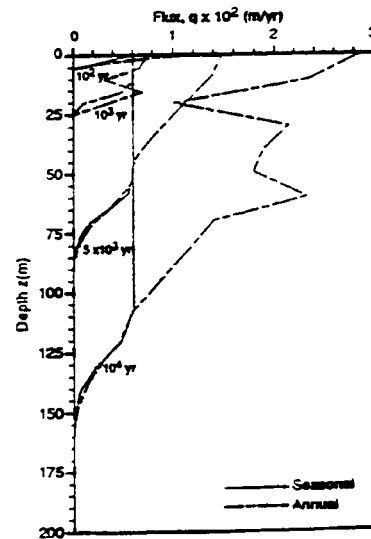
Figure 3b. Comparison of flux profiles at various time intervals for season and annual fluctuation of climatic parameters
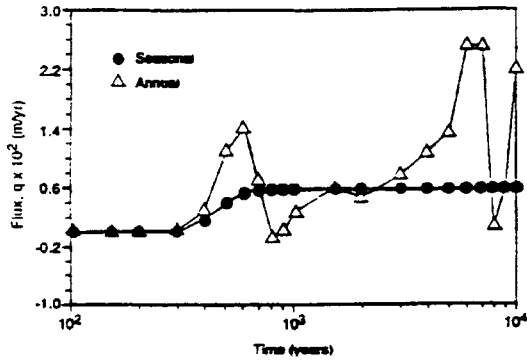
Figure 4a. Temporal variation of flux at 10 m for seasonal and annual fluctuation of climatic parameters
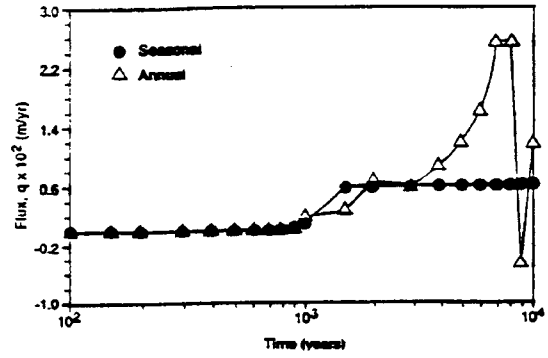
Figure 4b. Temporal variation of flux at 25 m for seasonal and annual fluctuation of climatic parameters
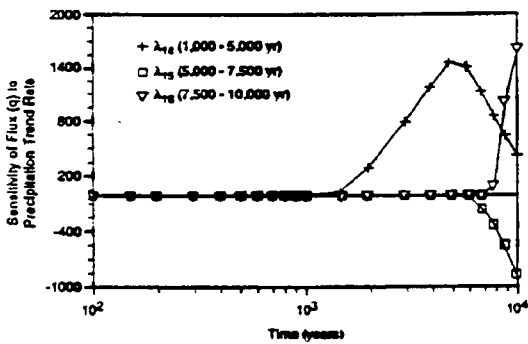
Figure 5a. Profiles of temporal variation of sensitivity of flux (q) to trend rate parameter λ_{1j}
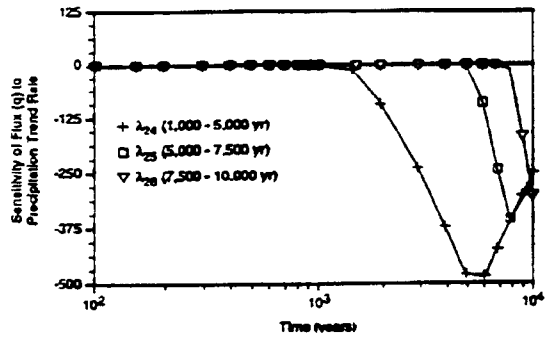
Figure 5b. Profiles of temporal variation of sensitivity of flux (q) to trend rate parameter λ_{2j}
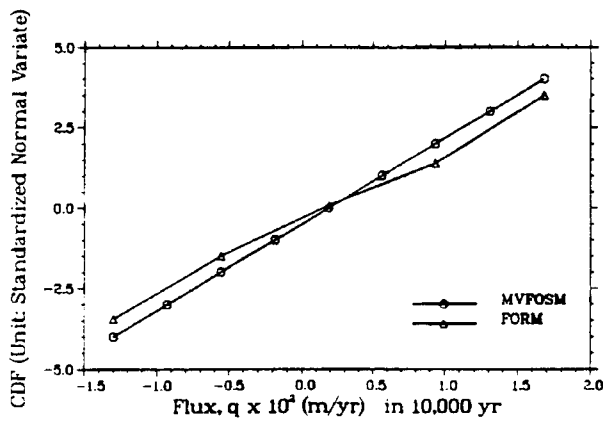
Figure 6a. Comparisons of CDF Analysis Results
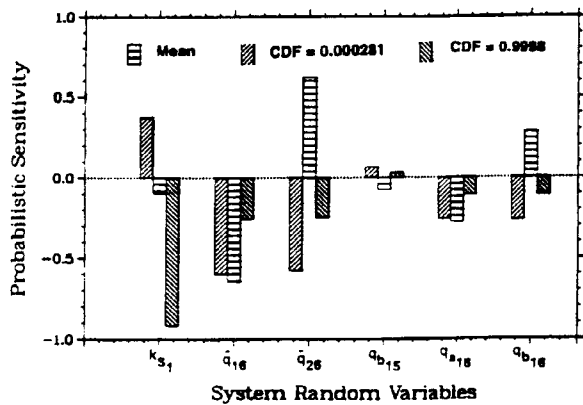
Figure 6b. Probabilistic Sensitivity Factors

GL.PEGHIAN - 12